

# Slow epidemic extinction in populations with heterogeneous infection rates

C. Buono,<sup>1</sup> F. Vazquez,<sup>2,3</sup> P. A. Macri,<sup>1</sup> and L. A. Braunstein<sup>1,4</sup>

<sup>1</sup>*Instituto de Investigaciones Físicas de Mar del Plata (IFIMAR)-Departamento de Física FCEyN-UNMDP-CONICET Funes 3350 (7600) Mar del Plata, Argentina.*

<sup>2</sup>*Max-Planck-Institut für Physik Komplexer Systeme  
Nöthnitzer Str. 38, D-01187 Dresden, Germany.*

<sup>3</sup>*Instituto de Física de Líquidos y Sistemas Biológicos UNLP-CONICET,  
Calle 59 Nro 789 (1900), La Plata Argentina.*

<sup>4</sup>*Center for Polymer Studies, Boston University,  
Boston, Massachusetts 02215, USA.*

## Abstract

We explore how heterogeneity in the intensity of interactions between people affects epidemic spreading. For that, we study the susceptible-infected-susceptible model on a complex network, where a link connecting individuals  $i$  and  $j$  is endowed with an infection rate  $\beta_{ij} = \lambda w_{ij}$  proportional to the intensity of their contact  $w_{ij}$ , with a distribution  $P(w_{ij})$  taken from face-to-face experiments analyzed in Cattuto *et al.* (PLoS ONE 5, e11596, 2010). We find an extremely slow decay of the fraction of infected individuals, for a wide range of the control parameter  $\lambda$ . Using a distribution of width  $a$  we identify two large regions in the  $a - \lambda$  space with anomalous behaviors, which are reminiscent of rare region effects (Griffiths phases) found in models with quenched disorder. We show that the slow approach to extinction is caused by isolated small groups of highly interacting individuals, which keep epidemic alive for very long times. A mean-field approximation and a percolation approach capture with very good accuracy the absorbing-active transition line for weak (small  $a$ ) and strong (large  $a$ ) disorder, respectively.

PACS numbers: 89.75.Hc, 05.40.-a, 87.19.X-, 02.50.Ey

Nowadays, much of the daily human activity is constantly being recorded by means of modern technologies such as Internet, GPS, mobile phones, blue-tooth and other electronic devices. The gathering and analysis of large amount of activity data have allowed to explore statistical features on people's behavior. In particular, recent studies have revealed interesting properties about how humans interact with each other, either by having conversations [1], or sexual contacts [2], or by means of mobile devices [3] or wireless communications [4]. Despite the fact that the type of interactions in these studies are quite different, they all found a common interaction pattern, that is, human contacts are very heterogeneous. This is consistent with a broad distribution of different magnitudes that quantify the timing of contacts, such as their duration, frequency and gaps. This diversity could eventually have an impact on propagation processes that involve human contact, such as the spreading of rumors or diseases.

In this letter we explore epidemic spreading on a population with heterogeneous interaction intensities. We use a distribution of intensities extracted from the pattern of contacts between participants of a conference [5], obtained in recent face-to-face (F2F) experiments [1]. For the spreading process we use the Susceptible-Infected-Susceptible (SIS) [6] dynamics on Erdős-Rényi (ER) networks [7], with infection rates across links that are proportional to the intensity of encounters.

As the infection rate increases, the SIS model [6] exhibits a transition, from an absorbing (disease-free) phase where the infection dies exponentially fast to an active (endemic) phase where the infection spreads over a large fraction of the population and becomes persistent. We find that the heterogeneity in the intensity of contacts introduces an intermediate absorbing region, in which the epidemic dies very slowly, as a stretched exponential or a power law in time. We experiment with other rate distributions and show that this slow approach to epidemic extinction is caused by the presence of small clusters composed by links with high interaction time, which remain infected for very long times. We also discuss analogies with the effects observed in models with quenched disorder [8].

While our results are mainly concerned with the decay of the infection in the epidemic-free phase, some related models [9–11] have focused, instead, on the disease prevalence within the endemic phase. Other studies have introduced heterogeneity at the individual level, by assigning power law intertime events [12, 13] or node-dependent infection rates [14]. In our model heterogeneity is at the interaction level, by means of link-dependent

infection rates.

*SIS dynamics with F2F disorder.* In the SIS model [6], each individual of a population can be either susceptible (healthy) or infected. Infected individuals transmit the disease to its susceptible neighbors in the network at a rate  $\nu$  and return to the susceptible state at a rate  $\gamma$ . The dynamics is controlled by the rescaled infection rate  $\lambda = \nu/\gamma$ . For  $\lambda$  above a critical value  $\lambda_c$ , even a small initial fraction of infected nodes is able to propagate the disease through the entire network (active phase), while for  $\lambda < \lambda_c$  the disease quickly dies out (absorbing phase), following an exponential decay in the number of infected nodes.

This model describes disease spreading in an ideal population where transmission rates between individuals are all the same. However, in real populations we expect interactions to be heterogeneous, having a broad range of intensities, as recently measured by analyzing mobiles phone data [3] and by means of person-to-person experiments [1]. In order to explore how the behavior of the SIS model is affected by the heterogeneity of interactions, we run simulations of the dynamics on ER networks with infection rates distributed according to the weight distribution  $P(w)$  of F2F experiments [1, 5] (see Fig. 1). In these experiments, participants of a three-day congress were asked to wear a *Radio Frequency Identification* device on their chest, so that when two persons were close and facing each other a relation of face-to-face proximity was registered. The weights  $w$  of Fig. 1 are defined as the total number of packets exchanged (or total contact time) between pairs of participants during the three days.

We are assuming that infection rates are proportional to the total time individuals are in contact with each other, as the likelihood of transmission increases with exposure time -longer contacts imply a higher risk of infection-. Therefore, we assign an *effective rate of infection*  $\beta_{ij} = \lambda w_{ij}$  between two individuals  $i$  and  $j$  that are connected by a link of weight  $w_{ij}$ , where  $\lambda$  is a free parameter that acts as a transformation scale of contact intensities into infection rates.

In Fig. 2 we show simulation results of the time evolution of the average density of infected individuals  $\rho$ , over many realizations of the SIS dynamics, starting from a configuration where a small fraction of nodes have been randomly infected, and with infection rates following the distribution of Fig. 1. All simulations in this article correspond, unless noted, to ER networks of mean degree  $\langle k \rangle = 4$  and  $N = 10^5$  nodes. We found that, besides the typical behavior observed in the active and exponential phases of the *clean* SIS

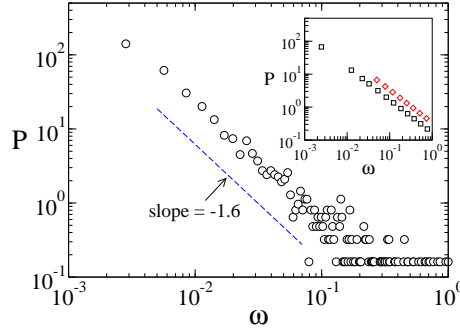


FIG. 1: Probability distribution of face-to-face contacts intensities (weights  $w$ ) of the 25th Chaos Communication Congress in Berlin, on a log-log scale. Intensity is defined as the total number of packages exchanged between two attendees, which is proportional to the contact duration. The large dispersion of the data reflects the large heterogeneity in the duration of contacts. Weights are rescaled to the interval  $[0, 1]$  for a better comparison with the theoretical distribution  $P(w) = 1/aw$  in the interval  $[e^{-a}, 1]$ , as shown in the inset for  $a = 6$  (squares) and  $a = 3$  (diamonds).

model (all infection rates are the same), there is an intermediate region between  $\lambda = 0.25$  and  $3.7$  with very slow relaxation to the absorbing state. The region  $2.0 \lesssim \lambda \lesssim 3.7$  is characterized by a power-law decay with a continuously varying exponent, while in the region  $0.25 \lesssim \lambda \lesssim 2.0$  the decay is faster than a power law but slower than exponential (see the inset of Fig. 2), and can be fitted by a stretched exponential.

*SIS with variable disorder strength.* In order to understand this phenomenon we explore the dynamics for different distributions of weights. We assign to each link  $ij$  a weight  $w_{ij} = e^{-ar_{ij}}$ , where  $r_{ij}$  is a random number taken from a uniform distribution in the interval  $[0, 1]$ , and  $a$  is a parameter that sets the range of  $w_{ij}$  in  $[e^{-a}, 1]$ . This method generates a power-law distribution  $P(w) = 1/aw$ . The parameter  $a$  controls the width of the distribution, and measures the heterogeneity or strength of disorder. In the inset of Fig. 1 we plot  $P(w)$  for  $a = 6$  and  $a = 3$ , which is intended to mimic the broad distribution of F2F contacts, even though the decay exponents are somewhat different.

The distribution of infection rates is given by

$$P(\beta) = \frac{1}{a\beta}, \quad \text{with } \beta \text{ in } [\lambda e^{-a}, \lambda]. \quad (1)$$

Notice that when  $a \rightarrow 0$  we recover the clean model where  $\beta_{ij} = \lambda$  for all  $ij$ . This kind

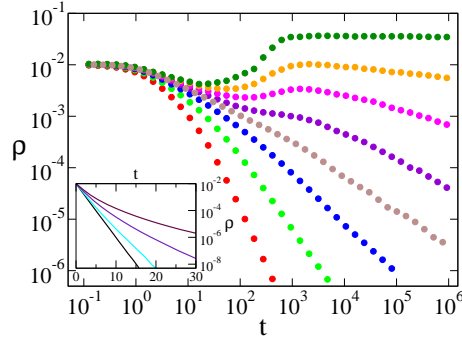


FIG. 2: Average density of infected nodes  $\rho$  vs time  $t$ , on a log-log scale, under the SIS dynamics on ER networks with  $\langle k \rangle = 4$  and  $N = 10^5$  nodes. The infection rate distribution  $P(\beta)$  corresponds to the weight distribution  $P(w)$  of Fig. 1, with  $\beta = \lambda w$ , for values of the control parameter  $\lambda = 3.9, 3.7, 3.6, 3.5, 3.4, 3.3, 3.0, 2.5$  (main plot) and  $\lambda = 1.5, 1.0, 0.5, 0.2$  (inset), from top to bottom.  $\rho$  decays as a power-law for  $2.0 \lesssim \lambda \lesssim 3.7$ , as a stretched exponential for  $0.25 \lesssim \lambda \lesssim 2.0$ , and as an exponential for  $\lambda \lesssim 0.25$ , as shown in the inset on a linear-log scale.

of disorder was already used in several works on complex networks [15, 16], where it was found that in the *strong disorder limit*  $a \rightarrow \infty$  [17], magnitudes such as the current flow [18] are highly affected, since links with very small weights are rarely traversed by the flow. In the same way, we expect that high-weight links facilitate the spreading of infections in our model, while low-weight links hinder the spreading.

Numerical simulations show that the behavior of  $\rho$  under the theoretical disorder given by Eq. (1) (not shown) is very similar to the one observed in Fig. 2 for the F2F disorder. In the  $a - \lambda$  phase diagram of Fig. 3 we summarize the different types of behaviors. Above the numerical transition line  $\lambda_c^{\text{num}}(a)$  denoted by the red circles we find the *active phase* (white), where  $\rho$  reaches a stationary value larger than zero, and below we find the *absorbing phase* where  $\rho$  decays to zero. For  $a = 0$  we recover the *clean* transition point  $\lambda_c^0 \equiv \lambda_c(a = 0) = 1/\langle k \rangle = 0.25$  of the clean model. The absorbing phase is divided into three regions. The *exponential region* (green), which appears for  $\lambda < \lambda_c^0$ , characterized by the decay  $\rho \sim e^{-\alpha t}$  of the clean model, the *weak effects region* (yellow) where we observe an stretched exponential behavior  $\rho \sim e^{-\alpha t^b}$  ( $b < 1.0$ ), and the *strong effects region* (orange), with a power law decay  $\rho \sim t^{-\gamma}$ . Exponents  $\alpha$ ,  $b$  and  $\gamma$  vary continuously with  $\lambda$  and  $a$ . We note that the pure stretched exponential decay is strictly observed just above the line  $\lambda = \lambda_c^0$ , while a smooth crossover to the pure power law behavior is found

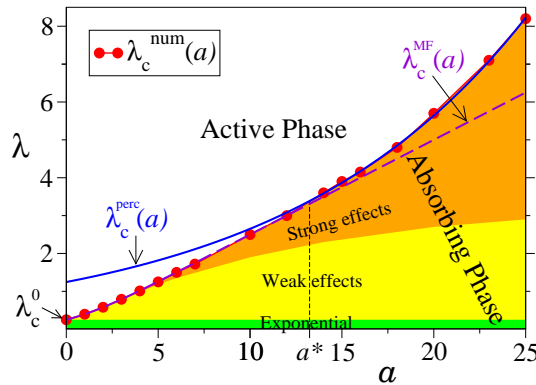


FIG. 3: Phase diagram of the SIS model with infection rate distribution  $P(\beta) = 1/a \beta$ , and  $\beta$  in  $[\lambda e^{-a}, \lambda]$ . Colored regions correspond to the absorbing phase: orange and yellow for the strong and weak effects regions, and green for the exponential decay region. The dashed and solid lines are the MF [Eq. (3)] and percolation [Eq. (6)] approximations, respectively, for the transition between the active and absorbing phases.

in the intermediate region.

In summary, the heterogeneity in infection rates induces a large new region inside the absorbing phase, in which the temporal evolution of  $\rho$  exhibits an anomalous slow decay. This is caused by the presence of exponentially small isolated regions in the network where the system is locally active, that is, with infection rates  $\beta_{ij} > \lambda_c^0$ , which are able to sustain the activity for very long times. To check this, we calculated the size distribution of clusters composed only by infected nodes  $n_I(s)$ , at a fixed large time. Results are shown in Fig. 4. Inside the weak and strong effects regions ( $\lambda = 0.75$  and  $1.4$ ),  $n_I(s)$  is close to an exponential, and the size of the largest cluster  $s_{\max}$  is much smaller than the network size  $N = 10^5$  (see inset of Fig. 4). Also, the values 0.27 and 0.70 of the average infection rates inside these clusters for  $\lambda = 0.75$  and  $1.4$ , respectively, show that the long-time activity is located inside *active clusters*, in which the average rate of infection  $\langle \beta \rangle > \lambda_c^0$ . For comparison, in the active phase ( $\lambda = 2.0$ ) is  $7600 \lesssim s_{\max} \lesssim 9500$ , indicating the spreading of the disease over a large fraction of the network.

Similar anomalous behaviors are found in models with disorder, given rise to the so-called Griffiths phases (GP) [8, 14, 19, 20]. The combination of exponentially rare regions in space that survive for exponentially long times results in an overall slowing down of the dynamics, as we show below. The long-time contribution of active clusters to  $\rho$  is

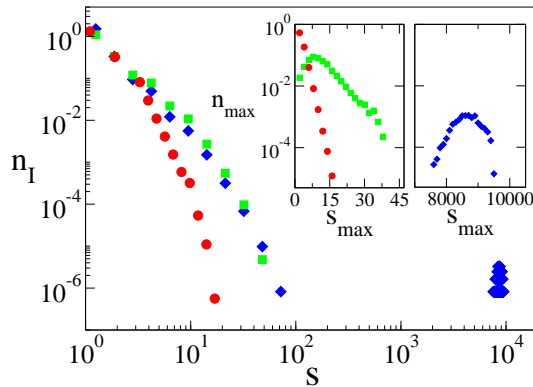


FIG. 4: Main: cluster size distribution of infected nodes  $n_I$  for  $a = 6$  and values of  $\lambda$  inside three different regions of Fig. 3:  $\lambda = 0.75$  (circles) and  $1.4$  (squares) in the weak and strong effects regions, and  $2.0$  (diamonds) in the active phase. Distributions correspond to snapshots of the network at fixed large times. The average infection rates inside each cluster are  $\langle\beta\rangle \simeq 0.27, 0.70$  and  $0.75$  for  $\lambda = 0.75, 1.4$  and  $2.0$ , respectively. Insets: size distribution of the largest cluster  $n_{\max}$  showing the appearance of a large component in the active phase.

estimated as

$$\rho \sim \int ds s P(s) e^{-t/\tau(s)}, \quad (2)$$

where  $P(s) \sim e^{-\tilde{p}s}$  [21] is the fraction of active clusters of size  $s$  and  $\tau(s)$  is the mean decay time of those clusters. By doing a saddle-point analysis, and using the finite-size scaling  $\tau(s) \sim e^{cs}$ , one arrives to the power-law decay  $\rho \sim t^{-\tilde{p}/c}$  (with logarithmic corrections) observed in the strong effects region of Fig. 3. The size of active clusters is of order two for  $\lambda$  just above  $\lambda_c^0$ , leading to exponentially weak effects of the form  $\rho \sim e^{-\alpha t^b}$  [8].

*Mean-field and percolation approaches.* Within a mean-field (MF) approximation,  $\rho$  evolves according to  $\dot{\rho} = -\rho + \lambda \langle w \rangle \langle k \rangle \rho (1 - \rho)$ , where  $\lambda \langle w \rangle = \lambda(1 - e^{-a})/a$  is the average infection rate, and  $\langle k \rangle (1 - \rho)$  is the average number of susceptible neighbors of an infected node. The stationary solutions  $\rho = 0$  and  $\rho = (\lambda - \lambda_c^{\text{MF}})/\lambda$  correspond to the absorbing and active phases, respectively, with the transition point at

$$\lambda_c^{\text{MF}}(a) = \frac{a}{\langle k \rangle (1 - e^{-a})}, \quad (3)$$

*Impurities*, in the form of low-weight links, locally reduce infection rates, thus the transition happens at a value  $\lambda_c^{\text{MF}}(a) > \lambda_c^0$ .

Expression (3) (dashed line in Fig. 3) is a very good estimate of  $\lambda_c^{\text{num}}(a)$  for  $a \lesssim 14$  (weak

disorder), but systematic deviations appear as  $a$  increases. Discrepancies arise because MF assumes that *all* links can spread the disease but, when  $a$  is large, a fraction of links have such small rates (inactive links) that infection never passes through them during the epidemic's life time, and thus the *effective* network for the spreading dynamics is diluted respect to the original network. When dilution is large enough the effective network gets fragmented into many small disconnected components and, as the disease cannot spread out of these components the active state is never reached. Therefore, the active-absorbing transition point for  $a$  large (strong disorder) corresponds to the *percolation threshold*. This occurs when the fraction of inactive nodes  $q$  (nodes attached only to inactive links) exceeds the critical value  $q_c$ . For ER networks with Poissonian degree distribution  $P_k = e^{-\langle k \rangle} \frac{\langle k \rangle^k}{k!}$  is

$$q = \sum_k l_1^k P_k = e^{-\langle k \rangle (1-l_1)}, \quad \text{where} \quad (4)$$

$$l_1 \equiv \int_{\lambda e^{-a}}^{\beta_m} P(\beta) d\beta = \frac{1}{a} \ln \left( \frac{\beta_m e^a}{\lambda} \right) \quad (5)$$

is the fraction of inactive links, and  $\beta_m$  is the largest infection rate that does not allow to transmit the disease. At the percolation threshold  $\langle k \rangle = (1 - q_c)^{-1}$  in the  $N \rightarrow \infty$  limit, thus  $q_c = \exp[(1 - q_c)^{-1} \ln(\beta_m e^a / \lambda_c^{\text{perc}}) / a - 1]$ , from where the percolation transition line is

$$\lambda_c^{\text{perc}}(a) = \beta_m q_c^{-a(1-q_c)}. \quad (6)$$

Using  $q_c = 0.7443$  for a network of size  $N = 10^5$  [22], expression (6) with  $\beta_m \simeq 1.2457$  is in excellent agreement with  $\lambda_c^{\text{num}}(a)$  for  $a \gtrsim 14$  (solid line in Fig. 3). The value of  $\beta_m$  is estimated from the crossover conditions  $\lambda_c^{\text{MF}}(a) = \lambda_c^{\text{perc}}(a)$  and  $\partial \lambda_c^{\text{MF}}(a) / \partial a = \partial \lambda_c^{\text{perc}}(a) / \partial a$  between the MF and percolation lines at the weak-strong disorder crossing point  $a = a^*$ . We obtain  $\beta_m = -[e \ln q_c]^{-1}$  and  $a^* = -[(1 - q_c) \ln q_c]^{-1}$  with  $a^* \simeq 13.243$  for the network used here.

*Summary and Conclusions.* In summary, the heterogeneity in the intensity of contacts between individuals induces a regime with extremely slow (power-law or stretched exponential) relaxation to epidemic extinction, akin to the slowing down found in systems with quenched disorder. This effect is very robust, as it was observed using an empirical distribution of contact durations in F2F experiments, as well as a theoretical distribution with variable width. While *temporal* heterogeneity, causality and bursty activity was found

to hinder spreading [11, 13], we showed here that *spatial* heterogeneity has the counter-balanced effect, making epidemic more persistence by slowing down its extinction. Once a group of highly interacting individuals gets infected, is able to continuously reinfect each other at a high rate, keeping the infection inside the group for very long times. Our founding can be used to design efficient mitigation strategies for the disease. For instance, moderating the activity of highly interacting people could dramatically speed up the final stage of the epidemic.

This work was financially supported by UNMdP and FONCyT (Pict 0293/2008). The authors thank Lucas D. Valdez for useful comments and discussions.

- 
- [1] C. Cattuto, W. V. den Broeck, A. Barrat, V. Colizza, J.-F. Pinton, and A. Vespignani, PLoS ONE **5**, e11596 (2010).
  - [2] B. Foxman, M. Newman, B. Percha, K. Holmes, and S. Aral, Sex Transm Dis **33**, 209 (2006).
  - [3] T. Karagiannis, J.-Y. L. Boudec, and M. Vojnovic, Mobicom **07**, 183 (2007).
  - [4] A. Scherrer, P. Borgnat, E. Fleury, J.-L. Guillaume, and C. Robardet, Computer Networks **52**, 2842 (2008).
  - [5] [Http://people.openbeacon.org/meri/openbeacon/sputnik/data/25c3](http://people.openbeacon.org/meri/openbeacon/sputnik/data/25c3).
  - [6] N. T. J. Bailey, *The Mathematical Theory of Infectious Diseases* (Griffin, London, 1975).
  - [7] P. Erdős and A. Rényi, Publications Mathematicae **6**, 290 (1959).
  - [8] T. Vojta, J. Phys. A: Math. Gen. **39**, R143 (2006).
  - [9] J. Stehlé et al., BMC Medicine **9**, 87 (2011).
  - [10] Z. Yang and T. Zhou, Phys. Rev. E **85**, 056106 (2012).
  - [11] M. Karsai, M. Kivelä, R. K. Pan, K. Kaski, J. Kertész, A.-L. Barabási, and J. Saramäki, Phys. Rev. E **83**, 025102(R) (2011).
  - [12] A. Vazquez, B. Rácz, A. Lukács, and A.-L. Barabási, Phys Rev Lett **98**, 158702 (2007).
  - [13] B. Min, K.-I. Goh, and A. Vazquez, Phys. Rev. E **83**, 036102 (2011).
  - [14] M. A. Muñoz, R. Juhász, C. Castellano, and G. Odor, Phys. Rev. Lett. **105**, 128701 (2010).
  - [15] L. A. Braunstein, S. V. Buldyrev, S. Havlin, and H. E. Stanley, Phys. Rev. E **65**, 056128

(2002).

- [16] C. Buono, C. Lagorio, P. A. Macri, and L. A. Braunstein, *Physica A* **391**, 4181 (2012).
- [17] M. Cieplak, A. Maritan, and J. R. Banavar, *Phys. Rev. Lett.* **76**, 3754 (1996).
- [18] Z. Wu, E. López, S. V. Buldyrev, L. A. Braunstein, S. Havlin, and H. E. Stanley, *Phys. Rev. E* **71**, 045101 (R) (2005).
- [19] F. Vazquez, J. A. Bonachela, C. Lopez, and M. A. Muñoz, *Phys. Rev. Lett.* **106**, 235702 (2011).
- [20] R. Martínez-García, F. Vazquez, C. López, and M. A. Muñoz, *Phys. Rev. E* **85**, 051125 (2012).
- [21] M. E. J. Newman, S. H. Strogatz, and D. J. Watts, *Phys. Rev. E* **64**, 026118 (2001).
- [22] Z. Wu, C. Lagorio, L. A. Braunstein, R. Cohen, S. Havlin, and H. E. Stanley, *Phys. Rev. E* **75**, 066110 (2007).